INTERNATIONAL JOURNAL OF NUMERICAL MODELLING: ELECTRONIC NETWORKS, DEVICES AND FIELDS
Int. J. Numer. Model. 2010; **23**:42–61
Published online 18 August 2009 in Wiley InterScience (www.interscience.wiley.com). DOI: 10.1002/jnm.724

Wave digital simulation of passive systems in linear state-space form

Karlheinz Ochs*,†

Department of Electrical Engineering and Information Technology/Communications Engineering, Ruhr-University, D-44780 Bochum, Germany

SUMMARY

This paper deals with wave digital modeling of passive state-space models. The set of differential equations must be of linear state-space form, but all parameters can be time-variant and/or nonlinear. For such state-space models, a canonical internally passive reference circuit is presented and used for deriving wave digital structures. In order to show the usability, special solutions for important basic linear time-variant models are compared with wave digital simulation results. Moreover, the wave digital modeling of a nonlinear and time-variant oscillator is discussed. Especially for a lossless oscillator an implementation is proposed, which preserves energy under finite-arithmetic conditions. This is verified by comparing simulation results with the analytical solution of a gravity pendulum. Copyright © 2009 John Wiley & Sons, Ltd.

Received 4 March 2009; Accepted 10 June 2009

KEY WORDS: wave digital modeling; passivity; nonlinear systems; differential equations

1. INTRODUCTION

Originally, the wave digital concept has been used for emulating classical filter networks by means of replacing the analog circuit by a digital signal processing system [1]. As has been shown, wave digital filters exhibit outstanding properties such as inherent stability, robustness, low coefficient sensitivity, and absence of parasitic oscillations or limit cycles, which are all guaranteed even under finite word-length conditions [2–4]. This concept has also successfully been applied to numerical solutions of ordinary differential equations by digital simulation of nonlinear circuits, even with chaotic behavior [5–8]. Parallel to this development, the concept has been extended to multidimensional wave digital filters in order to numerically integrate partial differential equations [9–11]. But it would be too superficial to regard the wave digital concept merely as a simulation tool. In contrast to a simulation being performed for a short time

*Correspondence to: Karlheinz Ochs, Department of Electrical Engineering and Information Technology/Communications Engineering, Ruhr-University, D-44780 Bochum, Germany.
†E-mail: ochs@ieee.org

period, an emulation generally is a continuously running real-time application, for example, if the wave digital model acts as an observer of a physical system [12, 13]. In this case, rounding errors cannot be neglected and we have to contemplate a computer architecture with finite arithmetic in order to achieve a reliable algorithm. This is of special importance in safety-critical applications, where a wave digital model facilitates a formal verification of the correctness of the program [14].

When it comes to wave digital modeling of a physical system, a typical starting point are the associated differential equations and the main task is to find an appropriate electrical circuit. In case of a passive physical system, it is aspired to synthesize an internally passive electrical circuit consisting of port-wise interconnected passive multiports only. A proper reference circuit represents the differential equation and has additionally a one-to-one corresponding realizable wave digital model, leading to an explicit algorithm, cf. [15].

Of course, the advantage of using a higher-order differential equation is a condensed formulation of the physical system, being liberated from its domain and thus possibly easier to interpret in terms of electrical quantities. But the crux of using a higher-order differential equation is that we have sacrificed the structural information of the physical system. Hence, it requires a lot of experience and intuition for deriving a proper reference circuit possessing structural information. Since there is no systematic approach, it is advised to inspect the physical system and the assumed idealizations from which the differential equation originates. Beyond that, it is sometimes necessary to do a deeper physical modeling in order to conceive a passive mathematical model for the system and to justify the usage of a modified differential equation afterwards, cf. [13].

The aim of this paper is to give a systematic approach for synthesizing a proper reference circuit if the passive system is described in a formally linear state-space form possibly having nonlinear and/or time-variant parameters. For this purpose, the paper is organized as follows: in the next section, the mathematical model of the differential equation system under consideration is introduced and a very few basic cases are briefly discussed, which are necessary for references later on. The third section recapitulates some passive multiports in order to derive a canonical and internally passive electrical circuit for a multiport resistance. These multiports are needed in the subsequent section for synthesizing a reference circuit of a state-space model. The fifth section concerns a wave digital implementation of the reference circuit. Here, solutions for some basic, but important, linear time-variant systems are presented, in order to verify the new method by means of simulations. In the sixth section, a second-order nonlinear differential equation is treated. As an example, the gravity pendulum is explicitly discussed and wave digital simulation results are compared with the analytical solution. Finally, a conclusion is drawn.

2. MATHEMATICAL MODEL

Let us consider a system with l input signals, m output signals, and n states being collected in the column vectors $\mathbf{x}(t)$, $\mathbf{y}(t)$, and $\mathbf{z}(t)$, respectively. This system is assumed to be described by a differential equation system in state-space form,

$$\dot{\mathbf{z}}(t) = \hat{\mathbf{A}}\mathbf{z}(t) + \hat{\mathbf{B}}\mathbf{x}(t) \tag{1a}$$

$$\mathbf{y}(t) = \hat{\mathbf{C}}\mathbf{z}(t) + \hat{\mathbf{D}}\mathbf{x}(t) \tag{1b}$$

DOI: 10.1002/jnm

where the dot denotes a derivative with respect to time t. All parameters are supposed to be real and possibly time-variant and/or even nonlinear. In particular, these parameters are the elements of the system matrix $\hat{\mathbf{A}}$, the input and output matrix $\hat{\mathbf{B}}$ and $\hat{\mathbf{C}}$, and the matrix $\hat{\mathbf{D}}$, which supplies feed-through terms. To be brief, the differential equation system is well posed and has a unique solution for $t \geqslant t_0$, when any initial state $z(t_0) = z_0$ is given at the initial instance t_0. In the sequel, we will restrict ourselves to a negative definite system matrix, i.e., we lay stress on a passive differential equation system, cf. [16–18]:

$$\hat{\mathbf{A}} + \hat{\mathbf{A}}^{\mathrm{T}} < \mathbf{0} \tag{2}$$

From literature on system theory, it is well known that this differential equation system can be analytically solved if all parameters are constant. Even in case of time-varying parameters there exists a closed form solution [19]:

$$\mathbf{z}(t) = \hat{\mathbf{\Phi}}(t, t_0)\mathbf{z}_0 + \int_{t_0}^{t} \hat{\mathbf{\Phi}}(t, \tau)\hat{\mathbf{B}}(\tau)\mathbf{x}(\tau)\,\mathrm{d}\tau \quad \text{for } t \geqslant t_0 \tag{3}$$

But we still encounter difficulties, because this solution depends on the so-called transition matrix $\hat{\mathbf{\Phi}}$, being generally sophisticated if not impossible to determine. Whereas we can resort to closed-form solutions for linear differential equation systems, there are only a few special cases if the state-space model (1) is nonlinear, where the nonlinearity is characterized by state-dependent parameters.

As it has been stated in the introduction, the aim is to emulate the state-space model by a wave digital model, rather than merely to numerically solve the associated differential equations. In order to verify some simulation results presented later on, the solution of some linear (time-variant) state-space models will be presented as they commonly occur, if we succeed in decoupling the differential equation system by means of a suited state transformation.

2.1. Linear scalar state-space model

As a first example we consider the state-space model

$$\dot{z}(t) = \hat{a}(t)\, z(t) \quad \text{with } z(t_0) = z_0 \tag{4}$$

For this plain initial state problem, the solution is easily obtained from a separation of the variables and integration of the resulting expressions:

$$z(t) = \varphi(t, t_0)\, z_0 \quad \text{with } \varphi(t, t') = \psi(t)\, \psi^{-1}(t') \quad \text{for } t \geqslant t_0 \tag{5}$$

Here, $\psi(t)$ is the exponential function of the integrated time-varying parameter:

$$\psi(t) = \psi(t_0)\, \exp\left(\int_{t_0}^{t} \hat{a}(\tau)\,\mathrm{d}\tau \right) \tag{6}$$

It is worth to emphasize that this solution holds also for complex-valued $\hat{a}$ and z.

2.2. Linear state-space model with two conjugate complex eigenvalues

From a physical point of view, a complex-valued state-space model seems to be somewhat artificial. That is why we will give an interpretation of the scalar complex-valued state-space model of the previous subsection in the form of a real differential equation system. To this end, we introduce a state vector by separating the real and imaginary part of the original state:

$$\mathbf{z} = [\mathrm{Re}\{z\}, \mathrm{Im}\{z\}]^{\mathrm{T}} \quad \text{and} \quad \mathrm{z}_0 = [\mathrm{Re}\{z_0\}, \mathrm{Im}\{z_0\}]^{\mathrm{T}} \tag{7}$$

DOI: 10.1002/jnm

This yields a state-space model with a real system matrix having the eigenvalues $\hat{a}$ and $\hat{a}^*$:

$$\dot{\mathbf{z}} = \hat{\mathbf{A}}\mathbf{z} \text{ with } \hat{\mathbf{A}} = \begin{bmatrix} \mathrm{Re}\{\hat{a}\} & -\mathrm{Im}\{\hat{a}\} \\ \mathrm{Im}\{\hat{a}\} & \mathrm{Re}\{\hat{a}\} \end{bmatrix} \tag{8}$$

The corresponding solution of this system can hassle-free be derived by separating the solution (5) into its real and imaginary part,

$$\mathbf{z}(t) = \hat{\mathbf{\Phi}}(t, t_0)\mathbf{z}_0 \text{ with } \hat{\mathbf{\Phi}}(t, t') = \mathbf{\Psi}(t)\mathbf{\Psi}^{-1}(t') \tag{9}$$

where

$$\mathbf{\Psi}(t) = \begin{bmatrix} \mathrm{Re}\{\psi(t)\} & -\mathrm{Im}\{\psi(t)\} \\ \mathrm{Im}\{\psi(t)\} & \mathrm{Re}\{\psi(t)\} \end{bmatrix} \tag{10}$$

has the structure of the system matrix.

2.3. Linear state-space model with equal eigenvalues and one linearly independent eigenvector

In the end, we examine the differential equation system

$$\dot{z}_\nu(t) = \begin{cases} \hat{a}(t)\, z_\nu(t) + \Omega z_{\nu+1}(t) & \text{for } \nu = 1, \ldots, n-1 \\ \hat{a}(t)\, z_n(t) & \text{for } \nu = n \end{cases} \quad \text{with } z_\nu(t_0) = z_{\nu 0} \tag{11}$$

$\Omega > 0$, and at least two states: $n \geqslant 2$. In this particular situation, all eigenvalues of the system matrix are equal to $\hat{a}$ and only one linearly independent eigenvector exists. By starting with the last differential equation and a backward substitution technique we obtain the solution

$$z_\nu(t) = \varphi(t, t_0) \sum_{\mu=\nu}^{n} \frac{[\Omega[t - t_0]]^{\mu-\nu}}{[\mu - \nu]!}\, z_{\mu 0} \text{ for } t \geqslant t_0 \tag{12}$$

One ascertains that the parameter $\hat{a}$ is not limited to be real and could also be complex valued. Using a similar line of arguments as in the previous subsection, we maintain the real system interpretation

$$\mathbf{z}_\nu(t) = \hat{\mathbf{\Phi}}(t, t_0) \sum_{\mu=\nu}^{n} \frac{[\Omega[t - t_0]]^{\mu-\nu}}{[\mu - \nu]!}\, \mathbf{z}_{\mu 0} \text{ for } t \geqslant t_0 \tag{13}$$

where $\mathbf{z}_\nu$ and $\mathbf{z}_{\mu 0}$ comprise the real and imaginary part of z_ν and $z_{\mu 0}$, respectively.

3. SOME MULTIPORTS

3.1. Ideal multiport gyrator and transformer

In this section, a multiport gyrator and a multiport transformer, which are needed for later purposes, are concisely recapitulated [16]. At first, we recall the voltage-current relations of the multiport gyrator depicted on the left of Figure 1:

$$\mathbf{u}(t) = -\hat{\mathbf{R}}_\mathrm{a}^\mathrm{T}\mathbf{j}(t) \text{ and } \mathbf{v}(t) = \hat{\mathbf{R}}_\mathrm{a}\mathbf{i}(t) \tag{14}$$

where $\hat{\mathbf{R}}_\mathrm{a}$ is the gyration matrix of dimension $m \times n$, i.e., the multiport gyrator has m ports on the primary and n ports on the secondary side. From the power balance

$$p(t) = \mathbf{i}^\mathrm{T}(t)\mathbf{u}(t) + \mathbf{j}^\mathrm{T}(t)\mathbf{v}(t) = 0 \tag{15}$$

DOI: 10.1002/jnm

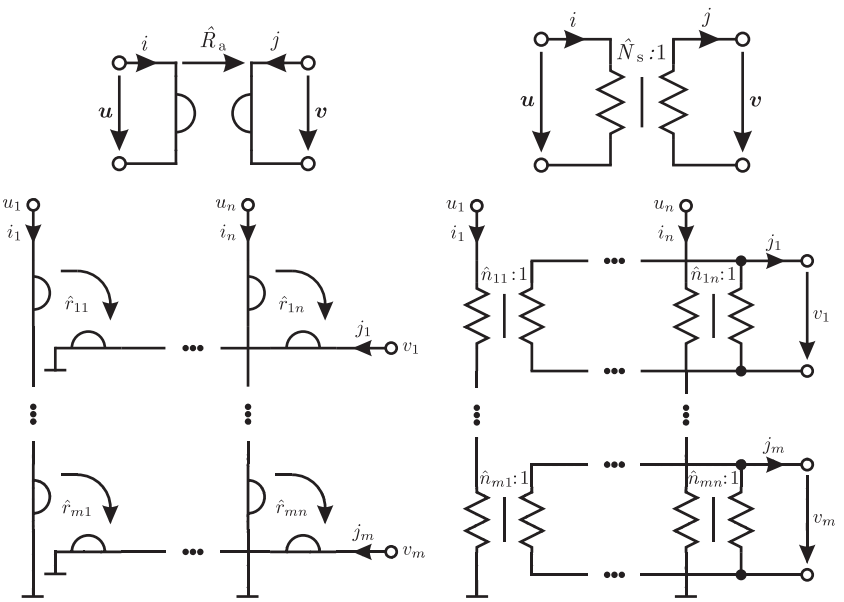

Figure 1. Top: Symbols of a multiport gyrator (left) and a multiport transformer (right). Bottom: Internally passive circuits for a multiport gyrator (left) and a multiport transformer (right).

we conclude, that—independent of its gyration matrix—this multiport is lossless. If we designate the entries of **u**, **i**, **v**, **j** by u_μ, i_μ, v_ν, and j_ν, respectively, the voltage-current relations can also be written as

$$u_\nu(t) = \sum_{\mu=1}^{m} u_{\mu\nu}(t), \quad v_{\mu\nu}(t) = \sum_{\nu=1}^{n} v_{\mu\nu}(t), \quad i_{\mu\nu}(t) = i_\nu(t), \quad j_{\mu\nu}(t) = j_\mu(t) \tag{16}$$

Here, the intermediate quantities are voltages and currents of *mn* twoport gyrators, where the gyrator resistances $\hat{r}_{\mu\nu}$ are the elements of the gyration matrix:

$$u_{\mu\nu}(t) = -\hat{r}_{\mu\nu} j_{\mu\nu}(t), \quad v_{\mu\nu}(t) = \hat{r}_{\mu\nu}\, i_{\mu\nu}(t) \tag{17}$$

Because of the voltage-current relations, one can easily verify the series connections of the gyrators shown in Figure 1. For the sake of clarity, a T-formed symbol indicates a zero-voltage reference level.

Secondly, we recall the multiport transformer shown on the right-hand side of Figure 1. Its voltage–current relations

$$\mathbf{u}(t) = \hat{\mathbf{N}}_s^{\mathrm{T}} \mathbf{v}(t) \ \text{ and } \ \mathbf{j}(t) = \hat{\mathbf{N}}_s \mathbf{i}(t) \tag{18}$$

imply losslessness being independent of the turns ratio matrix $\hat{\mathbf{N}}_s$:

$$p(t) = \mathbf{u}^{\mathrm{T}}(t)\mathbf{i}(t) - \mathbf{v}^{\mathrm{T}}(t)\mathbf{j}(t) = 0 \tag{19}$$

As it can be seen from Figure 1, the realization is based on *mn* twoport transformers with turns ratios $\hat{n}_{\mu\nu}$: 1, where $\hat{n}_{\mu\nu}$ is the associated element of $\hat{\mathbf{N}}_s$:

$$u_{\mu\nu}(t) = \hat{n}_{\mu\nu}\, v_{\mu\nu}(t), \quad j_{\mu\nu}(t) = \hat{n}_{\mu\nu}\, i_{\mu\nu}(t) \tag{20}$$

DOI: 10.1002/jnm

Again, the electrical quantities of the primary and secondary sides are denoted by u, i, v, and j, respectively. The interconnection network of the ideal transformers yields the relations

$$u_\nu(t) = \sum_{\mu=1}^{m} u_{\mu\nu}(t), \quad j_\mu(t) = \sum_{\nu=1}^{n} j_{\mu\nu}(t), \quad i_{\mu\nu}(t) = i_\nu(t), \quad v_{\mu\nu}(t) = v_\mu(t) \tag{21}$$

in accordance to the voltage–current relation of the multiport transformer. Apparent from that, the primary sides of the ideal twoport transformers of each column are in series and the secondary sides of each row are in parallel.

3.2. Multiport resistance

The goal of this section is to derive an internally passive electrical circuit for a multiport resistance, which has a resistance matrix being a positive matrix function [16]:

$$\mathbf{u} = \hat{\mathbf{Z}}\mathbf{i} \text{ with } \hat{\mathbf{Z}} + \hat{\mathbf{Z}}^{\mathrm{T}} > 0 \tag{22}$$

Note that, $\hat{\mathbf{Z}}$ is not constrained to be constant, i.e. $\hat{\mathbf{Z}}$ can be time-variant and/or even nonlinear. For the synthesis of an internally passive electrical circuit, the resistance matrix will be decomposed into its antimetric (skew-symmetric) and symmetric part

$$\hat{\mathbf{Z}} = \hat{\mathbf{Z}}_{\mathrm{a}} + \hat{\mathbf{Z}}_{\mathrm{s}} \text{ with } \hat{\mathbf{Z}}_{\mathrm{a}} = -\hat{\mathbf{Z}}_{\mathrm{a}}^{\mathrm{T}}, \hat{\mathbf{Z}}_{\mathrm{s}} = \hat{\mathbf{Z}}_{\mathrm{s}}^{\mathrm{T}} \tag{23}$$

which reflects a series connection of two n-ports,

$$\mathbf{u} = \mathbf{u}_{\mathrm{a}} + \mathbf{u}_{\mathrm{s}}, \quad \mathbf{u}_{\mathrm{a}} = \hat{\mathbf{Z}}_{\mathrm{a}}\mathbf{i}, \mathbf{u}_{\mathrm{s}} = \hat{\mathbf{Z}}_{\mathrm{s}}\mathbf{i} \tag{24}$$

Consequently, it remains to find internally passive realizations for these two multiports. Since the consumed power depends on the symmetric part only,

$$p(t) = \mathbf{i}^{\mathrm{T}}(t)\hat{\mathbf{Z}}\mathbf{i}(t) = \mathbf{i}^{\mathrm{T}}(t)\hat{\mathbf{Z}}_{\mathrm{s}}\mathbf{i}(t) \geqslant 0 \tag{25}$$

it is evident that $\hat{\mathbf{Z}}_{\mathrm{s}}$ comprises possible losses whereas $\hat{\mathbf{Z}}_{\mathrm{a}}$ belongs to a lossless multiport. If we synthesize an electrical circuit for the resistance matrix, we attain an alternative representation of the parameters: The values of the electrical elements take the place of the elements of $\hat{\mathbf{Z}}$. For the sake of efficiency, we appreciate a canonical electrical circuit with n^2 parameters.

3.2.1. Multiport with antimetric resistance matrix. In order to synthesize a multiport with antimetric resistance matrix, we write this matrix as a difference of a real matrix $\hat{\mathbf{R}}_{\mathrm{a}}$ and its transpose:

$$\hat{\mathbf{Z}}_{\mathrm{a}} = \hat{\mathbf{R}}_{\mathrm{a}} - \hat{\mathbf{R}}_{\mathrm{a}}^{\mathrm{T}} \tag{26}$$

Moreover, by choosing a strict lower triangular matrix,

$$\hat{r}_{\mu\nu} = 0 \text{ for } \mu < \nu \tag{27}$$

we incorporate the fact that a skew-symmetric matrix has $n[n-1]/2$ independent elements. In view of Equation (14), the voltage vector

$$\mathbf{u}_{\mathrm{a}}(t) = \hat{\mathbf{R}}_{\mathrm{a}}\mathbf{i}(t) - \hat{\mathbf{R}}_{\mathrm{a}}^{\mathrm{T}}\mathbf{i}(t) \tag{28}$$

describes the gyrator multiport of Figure 1, where all ports in column ν are in series with those of row ν. If we additionally take all resulting short-circuits from gyrators with vanishing gyration resistance into account, we achieve the internally passive electrical circuit of Figure 2.

DOI: 10.1002/jnm

3.2.2. Multiport with symmetric resistance matrix. It remains to synthesize an internally passive electrical circuit for the multiport with symmetric resistance matrix, having $n[n+1]/2$ degrees of freedom. Owing to Equation (25), this matrix is positive definite and we can make use of a Cholesky decomposition

$$\hat{\mathbf{Z}}_{\mathrm{s}} = \hat{\mathbf{N}}_{\mathrm{s}}^{\mathrm{T}} \hat{\mathbf{R}}_{\mathrm{s}} \hat{\mathbf{N}}_{\mathrm{s}} \tag{29}$$

From an electrical point of view, this decomposition describes n decoupled positive resistances

$$\mathbf{v}(t) = \hat{\mathbf{R}}_{\mathrm{s}}\, \mathbf{j}(t) \quad \text{with } \hat{\mathbf{R}}_{\mathrm{s}} = \mathrm{diag}(\hat{r}_v) \tag{30}$$

being interconnected to the secondary side of a multiport transformer, cf. (18). Here, $\hat{\mathbf{N}}_{\mathrm{s}}$ is a regular lower triangular $[n \times n]$-matrix with ones on its main diagonal:

$$\hat{n}_{\mu v} = \begin{cases} 1 & \text{for } \mu = v \\ 0 & \text{for } \mu < v \end{cases} \tag{31}$$

The corresponding electrical circuit is depicted in Figure 2, where in comparison to the multiport transformer of Figure 1, all ideal transformers with turns ratio 0:1 have been replaced by a short-circuit and an open-loop for the primary and secondary side, respectively. Aside from that, all ideal transformers with turns ratio 1:1 have been reduced to parallel connections.
On the one hand, the Cholesky decomposition preserves the number of parameters and leads, on the other hand, to n decoupled elementary inequalities for passivity:

$$\hat{r}_v > 0 \quad \text{for } v = 1, \ldots, n \tag{32}$$

Without sacrificing internal passivity, some resistances of the electrical circuit could also be zero so that we have a positive semidefinite resistance matrix. If a resistance vanishes, for example

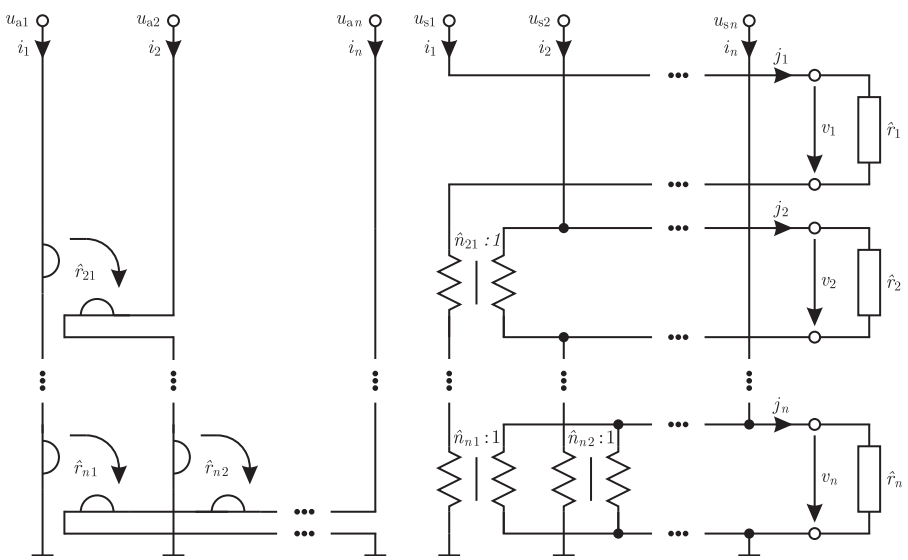

Figure 2. Canonical internally passive circuits for an antimetric and a symmetric multiport resistance, respectively.

DOI: 10.1002/jnm

$\hat{r}_\mu = 0$, all the associated transformers in row μ of Figure 2 are short-circuited and the corresponding turns ratios are arbitrary.

4. REFERENCE CIRCUIT FOR THE STATE-SPACE MODEL

4.1. Electrical interpretation

The treatment of the differential equation system in state-space form is closely related to the approach for the linear equation system (22). The extension to differential equations consists of an introduction of n energetic elements in order to reproduce the differential operators. For this purpose, it is sufficient to use n decoupled normalized inductances. As shown in Figure 3 (left), the vector $\mathbf{z}$ comprises the currents through the inductances and the derivative $\dot{\mathbf{z}}$ contains the corresponding voltages. The electrical circuit is supplied by l ideal voltage sources $\mathbf{x}(t)$ and provides m output voltages $\mathbf{y}(t)$. Furthermore, this realization is based on a multiport resistance with resistance matrix $-\hat{\mathbf{A}}$, a multiport gyrator with the gyration resistance matrix $\hat{\mathbf{C}}$ and two multiport transformers, whose turns ratios depend on the matrices $\hat{\mathbf{B}}$ and $\hat{\mathbf{D}}$, respectively. Since there is no load at the output terminals, the currents on the secondary side and thus the voltages on the primary side of the gyrator multiport vanish.

In order to decouple this electrical circuit in accordance to (1a) and (1b), we combine the transformers and voltage sources to controlled ideal voltage sources. Moreover, the secondary side of the gyrator multiport can also be replaced by controlled ideal voltage sources, whereas its primary side can be neglected. This way, we obtain the electrical circuits of Figure 3 (right), which represent the differential and the algebraic equations of the state space model.

4.2. An externally passive electrical circuit

From an electrical point of view, we are always interested in meaningful physical units. To this end, the state vector and its derivative are replaced by the vectors

$$\mathbf{i}(t) = \mathbf{z}(t) \quad \text{and} \quad \mathbf{u}(t) = \ell\dot{\mathbf{z}}(t) \tag{33}$$

containing currents and voltages of n decoupled identical positive inductances ℓ:

$$\mathbf{u}(t) = \mathbf{L}\frac{\mathrm{d}}{\mathrm{d}t}\,\mathbf{i}(t) \quad \text{with } \mathbf{L} = \mathbf{1}\ell \tag{34a}$$

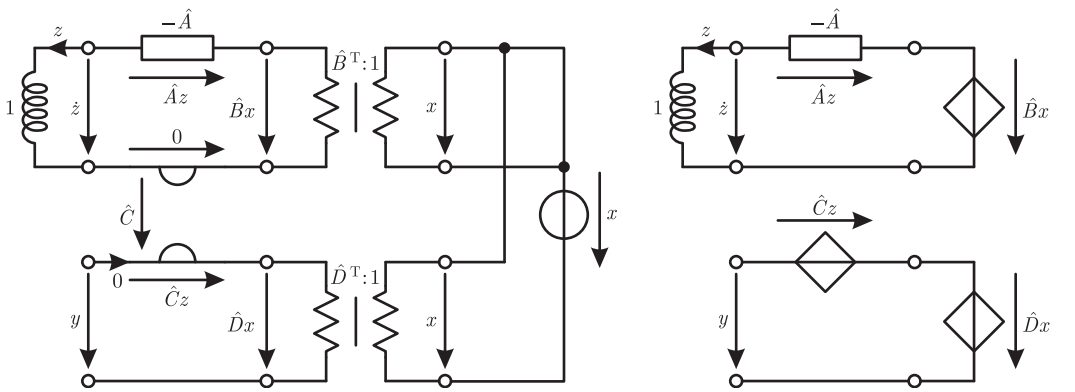

Figure 3. Electrical representations of the state-space model (1).

DOI: 10.1002/jnm

Consequently, the algebraic equations are

$$\mathbf{u}(t) = -\hat{\mathbf{Z}}\mathbf{i}(t) + \ell\,\hat{\mathbf{B}}\mathbf{x}, \quad \hat{\mathbf{Z}} = -\ell\hat{\mathbf{A}} \tag{34b}$$

where $\hat{\mathbf{Z}}$ is the resistance matrix of dimension $n \times n$. In order to have an externally passive electrical circuit $\hat{\mathbf{Z}}$, must necessarily be a positive matrix function or rather the system matrix must satisfy Equation (2). It is worth to emphasize that the usage of inductances does not limit this approach in any way. Of course, one may consider capacitances as well, but such considerations inevitably lead also to a positive admittance or hybrid matrix function [16].

4.3. A canonical internally passive electrical circuit

Starting from the merely externally passive electrical circuit, we obtain with the aid of Section 3.2 the internally passive electrical circuit in Figure 4. In order to create resistive voltage sources, we have transformed the ideal voltage sources on the secondary side of the transformer multiport, for which the source voltages have to multiplied with the transposed inverse of $\hat{\mathbf{N}}_\mathrm{s}$:

$$\mathbf{e} = \ell\,\hat{\mathbf{N}}_\mathrm{s}^{-\mathrm{T}}\hat{\mathbf{B}}\mathbf{x} \tag{35}$$

As a result, we have n decoupled normalized inductances and n resistive voltage sources, between those a nonenergic multiport is located. The latter is represented by an ideal transformer and a gyrator multiport and therefore divided into a reciprocal and a non-reciprocal part. The voltages–currents relations of this multiport can advantageously be formulated in dependence of a chain matrix:

$$\begin{bmatrix}\mathbf{u}\\ \mathbf{i}\end{bmatrix} = \hat{\mathbf{K}}\begin{bmatrix}\mathbf{v}\\ \mathbf{j}\end{bmatrix}, \quad \hat{\mathbf{K}} = \begin{bmatrix}\hat{\mathbf{N}}_\mathrm{s}^{\mathrm{T}} & -\hat{\mathbf{Z}}_\mathrm{a}\,\hat{\mathbf{N}}_\mathrm{s}^{-1}\\ \mathbf{0} & \hat{\mathbf{N}}_\mathrm{s}^{-1}\end{bmatrix} \tag{36}$$

Additionally, if we take the loop equations

$$\mathbf{e} = \mathbf{v} + \hat{\mathbf{R}}_\mathrm{s}\,\mathbf{j} \tag{37}$$

into account, we easily check that the electrical circuit indeed represents the differential Equations (1a) of the underlying state-space model.

5. WAVE DIGITAL MODELING

The internally passive electrical circuit of Figure 4 is now used for a wave digital modeling, in order to emulate the physical system described by the differential equation system. But to become acquainted with the complete wave digital theory is beyond the scope of this paper and the interested reader must be referred to the literature [3]. Hence, we restrict ourselves to the essential steps of wave digital modeling: First of all, the differential Equations (34a) of the

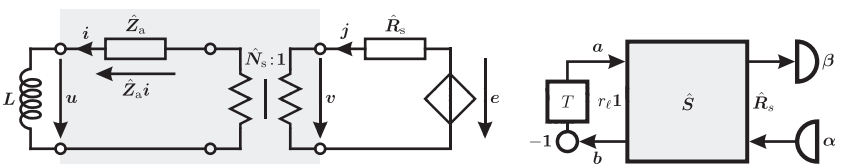

Figure 4. Electrical circuit of a state-space model and its draft for a wave digital modeling.

DOI: 10.1002/jnm

inductances can numerically be integrated by applying the trapezoidal rule:

$$\mathbf{i}(t) = \mathbf{i}(t-T) + \frac{T}{2\ell}[\mathbf{u}(t) - \mathbf{u}(t-T)] \text{ with } T>0 \tag{38}$$

where T is the step size of the integration method. In view of Equation (34b), this results in an implicit equation at an instance t, because the currents and voltages depend on each other. Now, if we choose

$$r_\ell = 2\ell/T \tag{39}$$

for all port resistances of the inductances and introduce the so-called power waves

$$\begin{bmatrix}\mathbf{b}\\ \mathbf{a}\end{bmatrix} = \mathbf{T}_\ell \begin{bmatrix}\mathbf{u}\\ \mathbf{I}\end{bmatrix}, \quad \mathbf{T}_\ell = \frac{1}{2\sqrt{r_\ell}}\begin{bmatrix}\mathbf{1} & -r_\ell\mathbf{1}\\ \mathbf{1} & r_\ell\mathbf{1}\end{bmatrix} \tag{40}$$

we achieve an explicit difference equation

$$\mathbf{a}(t) = -\mathbf{b}(t-T) \tag{41}$$

On the opposite side of the nonenergic multiport, the resistive voltage sources are interconnected. In terms of the port resistance matrix $\hat{\mathbf{R}}_\mathrm{s} = \hat{\mathbf{G}}_\mathrm{s}^{-1}$ and the power waves

$$\begin{bmatrix}\boldsymbol{\beta}\\ \boldsymbol{\alpha}\end{bmatrix} = \hat{\mathbf{T}}_\mathrm{s}\begin{bmatrix}\mathbf{v}\\ \mathbf{j}\end{bmatrix}, \quad \hat{\mathbf{T}}_\mathrm{s} = \frac{1}{2}\begin{bmatrix}\hat{\mathbf{G}}_\mathrm{s}^{1/2} & -\hat{\mathbf{R}}_\mathrm{s}^{1/2}\\ \hat{\mathbf{G}}_\mathrm{s}^{1/2} & \hat{\mathbf{R}}_\mathrm{s}^{1/2}\end{bmatrix} \text{ with } \hat{\mathbf{R}}_\mathrm{s}^{1/2} = \mathrm{diag}(\sqrt{\hat{r}_1}, \ldots, \sqrt{\hat{r}_n}) \tag{42}$$

Equation (37) becomes:

$$\boldsymbol{\alpha}(t) = \hat{\mathbf{G}}_\mathrm{s}^{1/2}\,\mathbf{e}(t)/2 \tag{43}$$

Figure 4 shows the resulting wave digital structure of the reference circuit, which is merely separated according to the inductances, the resistive controlled voltage sources, and the remaining nonenergic multiport. The latter obeys in view of Equation (36) the equations

$$\begin{bmatrix}\mathbf{b}\\ \mathbf{a}\end{bmatrix} = \mathbf{T}_\ell\hat{\mathbf{K}}\hat{\mathbf{T}}_\mathrm{s}^{-1}\begin{bmatrix}\boldsymbol{\beta}\\ \boldsymbol{\alpha}\end{bmatrix}, \quad \begin{bmatrix}\mathbf{b}\\ \boldsymbol{\beta}\end{bmatrix} = \hat{\mathbf{S}}\begin{bmatrix}\mathbf{a}\\ \boldsymbol{\alpha}\end{bmatrix} \tag{44}$$

where $\hat{\mathbf{S}}$ denotes the scattering matrix. Evidently, the structure remains unchanged if $\mathbf{e}(t) = \mathbf{0}$, being equivalent to $\boldsymbol{\alpha}(t) = \mathbf{0}$. On this account, it is sufficient to derive the wave digital model of the free system and to incorporate sources afterwards.

For a wave digital synthesis of the nonenergic multiport, one may directly use the reference circuit. Unfortunately, this approach is not always successful, because in general we get delay-free directed loops. In order to perceive this, let us synthesize a one-to-one corresponding wave digital structure of the circuit in Figure 5 by realizing series and parallel connections by series and parallel adaptors, respectively. As it is shown in the same figure, the resulting wave digital structure contains two delay-free directed loops, which represent implicit equations. Of course, one may numerically solve these implicit equations by an appropriate iteration method but this significantly reduces the efficiency of the algorithm.

An efficient wave digital algorithm requires a realizable wave digital structure [15] that is free of delay-free directed loops. To this end, one may apply a Householder factorization or a series of Givens rotations to the scattering matrix $\hat{\mathbf{S}}$ of the nonenergic multiport [20, 21]. The disadvantage of this approach is the computation effort of the resulting wave digital structure, with quadratically increasing complexity. Hence, the wave digital structure should be analyzed

DOI: 10.1002/jnm

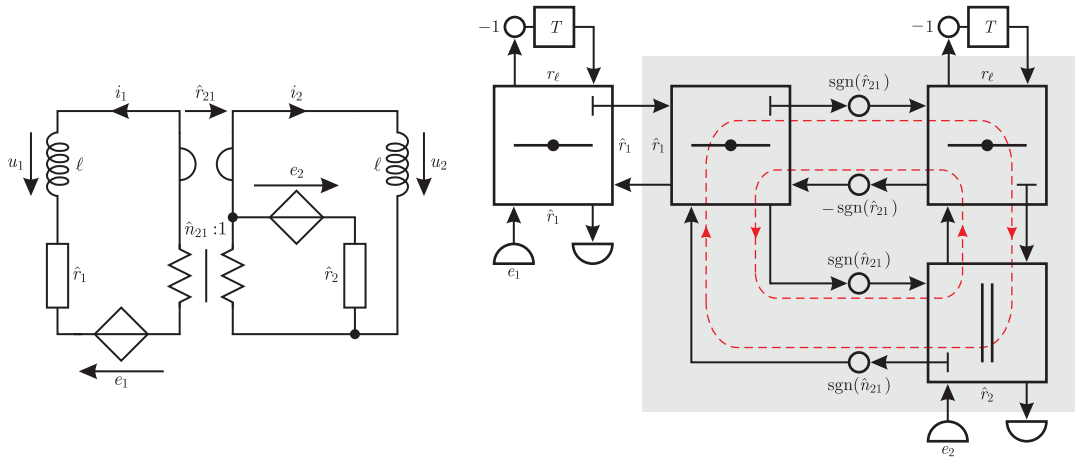

Figure 5. Left: Electrical circuit of a state-space model with two states. Right: Corresponding wave digital structure containing delay-free directed loops.

before, in order to realize as many as possible series and parallel connections and to find all remaining minimal nonrealizable substructures, cf. [22]. In Figure 5, the wave digital fourport has already been decomposed into a series adaptor with reflection-free port and a gray-shaded nonrealizable threeport, which can be realized by Householder factorization of its scattering matrix.

Although this preprocessing combined with a factorization of the associated scattering matrices of the nonrealizable substructures provides an explicit algorithm, the formulas of the resulting multiplier coefficients in dependence of the state-space parameters are more or less bulky. For that reason, some basic state-space models will be considered in the next subsections and efficient wave digital models will be derived.

5.1. Scalar wave digital model

The scalar state-space model coincides with a series connection of an inductance and a resistive source. The choice $r_\ell = 2\ell/T$ for the port resistance leads straightly to the simple wave digital structure of Figure 6. It is remarkable that this realization is not limited to a real-valued state-space model. For this reason, let us consider the complex-valued initial state problem

$$\hat{a}(t) = \frac{-\sigma}{1+e^{\sigma t}} + j\frac{-k\Omega}{1+\Omega^2 t^2} \Rightarrow \psi(t) = \frac{1+e^{-\sigma t}}{e^{jk\ \arctan(\Omega t)}} = \frac{1+e^{-\sigma t}}{[1+\Omega^2 t^2]^{k/2}}\,[1-j\Omega t]^k \tag{45}$$

with $k \in \mathbb{N}$ and $\Omega, \sigma > 0$.

The wave digital simulation results of the unforced system, with $k = 16$, $\Omega = \sigma = 1/\mathrm{s}$, and initial current $i(0) = 1\mathrm{A}$, are shown in Figure 7. They have a relative error of less than 1% at a step size $T = 1\,\mathrm{ms}$.

Note that arctan is monotonically increasing from zero to $\pi/2$ and implies a limited number of cycles because the phase of the solution traverses the interval $[0, -2\pi k/4)$. This circumstance is visualized by the trajectory depicted at the right-hand side of Figure 7: Starting from the initial

DOI: 10.1002/jnm

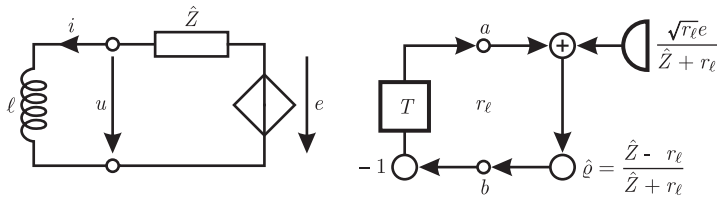

Figure 6. An electrical circuit and its wave digital realization for a scalar state-space model.

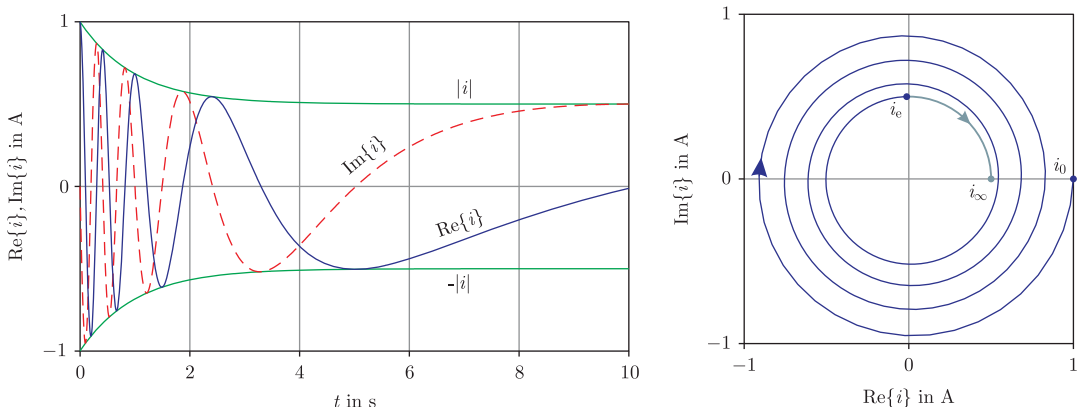

Figure 7. Wave digital simulation results: the real and imaginary part of the current (left) and their trajectory (right).

value $i_0 = i(0)$ the current reaches the point $i_e = i(t_e)$. From this instance $t_e = 10\,\text{ms}$, the trajectory moves on the thin line towards

$$\lim_{t\to\infty} i(t) = i_\infty = i_0/2 \tag{46}$$

5.2. *Wave digital model with two conjugate complex eigenvalues*

An example of a real system with two conjugate complex eigenvalues results, if the complex-valued initial state problem of the previous subsection is separated into its real and imaginary part. For this purpose, we multiply the real-valued system matrix of Equation (8) by $-\ell$ in order to obtain the associated resistance matrix having

$$\hat{\mathbf{Z}}_\text{s} = \begin{bmatrix} \hat{r}_1 + \hat{n}_{21}^2\hat{r}_2 & \hat{n}_{21}\hat{r}_2 \\ \hat{n}_{21}\hat{r}_2 & \hat{r}_2 \end{bmatrix} \text{ and } \hat{\mathbf{Z}}_\text{a} = \begin{bmatrix} 0 & -\hat{r}_{21} \\ \hat{r}_{21} & 0 \end{bmatrix}$$

as its symmetric and antimetric part, respectively, from which we deduce the electrical elements

$$\hat{r}_1 = \hat{r}_2 = -\ell\text{Re}\{\hat{a}\},\quad \hat{n}_{21} = 0,\quad \hat{r}_{21} = -\ell\text{Im}\{\hat{a}\} \tag{47}$$

The corresponding wave digital structure is shown in Figure 8, with port resistances $r_\ell = 2\ell/T$, $\hat{r}'_2 = \hat{r}_2 + r_\ell$, and $\hat{r}'_1 = \hat{r}_{21}^2/\hat{r}'_2$.

DOI: 10.1002/jnm

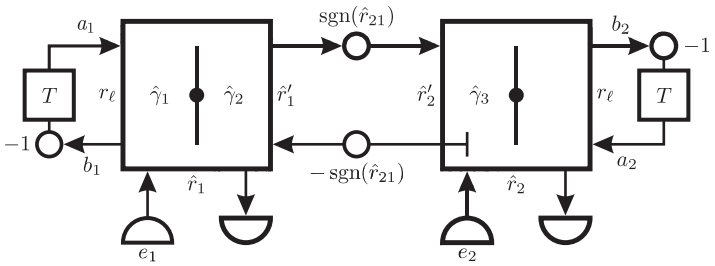

Figure 8. A wave digital structure for a real state-space model with two states and $\hat{n}_{21} = 0$.

5.3. Wave digital model with equal eigenvalues and one linearly independent eigenvector

Next, we examine the initial state problem (11), with the system matrix

$$\hat{\mathbf{A}} = \hat{a}\mathbf{1} + \Omega\mathbf{J} \quad \Leftrightarrow \quad \hat{\mathbf{Z}} = -\ell\hat{a}\mathbf{1} - \ell\Omega\mathbf{J} \tag{48}$$

where J is a Jordan block with vanishing main diagonal elements and the positive constant Ω has the physical unit of a frequency. From the antimetric part of the resistance matrix $\hat{\mathbf{Z}}$, we conclude

$$\hat{\mathbf{R}}_\mathrm{a} = r_\mathrm{a}\mathbf{J}, \quad \text{with } r_\mathrm{a} = \ell\Omega/2 \tag{49}$$

As a consequence, all gyration resistances of the first column in Figure 2 are identical $\hat{r}_{\mu 1} = r_\mathrm{a}$, whereas all other gyrator resistances vanish and the associated gyrators degenerate to short-circuits on both sides. Since the symmetric part of $\hat{\mathbf{Z}}$ is a tridiagonal matrix, one can find the turns ratios:

$$\hat{n}_{\mu\nu} = \begin{cases} -r_a/\hat{r}_\mu & \text{for } \nu = \mu - 1 \\ 0 & \text{for } \nu < \mu - 1 \end{cases} \quad \text{with } \mu = 2, \ldots, n \tag{50}$$

For the electrical circuit of Figure 2, this implies $n-1$ remaining ideal transformers, because all transformers with turns ratio 0:1 degenerate to short-circuits and open-loops on their primary and secondary sides, respectively. After somewhat lengthy but elementary computations one can deduce the recurrence formula

$$\hat{r}_{\mu-1} = \hat{r}_n - r_a^2/\hat{r}_\mu \ \text{ for } \mu = 2, \ldots, n \text{ with } \hat{r}_n = -\ell\hat{a} \tag{51}$$

Even though we have determined all devices of the electrical circuit, we know from an earlier discussion that a straightforward application of the wave digital concept leads to a realization, which generally contains undesired delay-free directed loops, cf. Figure 5. On this account, a method based on a direct synthesis of the resistance matrix

$$\hat{\mathbf{Z}} = \hat{r}_n\mathbf{1} - 2r_\mathrm{a}\mathbf{J} \tag{52}$$

is used here. If we choose all port resistances equal to $\hat{r}_n$, the scattering matrix reads:

$$\hat{\mathbf{S}}' = [\hat{\mathbf{Z}} - \hat{r}_n\mathbf{1}][\hat{\mathbf{Z}} + \hat{r}_n\mathbf{1}]^{-1} = \sum_{\nu=1}^{n-1} \hat{\mathbf{S}}_J^\nu \ \text{ with } \hat{\mathbf{S}}_J = -\hat{\varrho}\mathbf{J} \text{ and } \hat{\varrho} = \frac{r_\mathrm{a}}{\hat{r}_\mathrm{n}} \tag{53}$$

The special structure of the scattering matrix allows a direct wave digital implementation, cf. Figure 9.

DOI: 10.1002/jnm

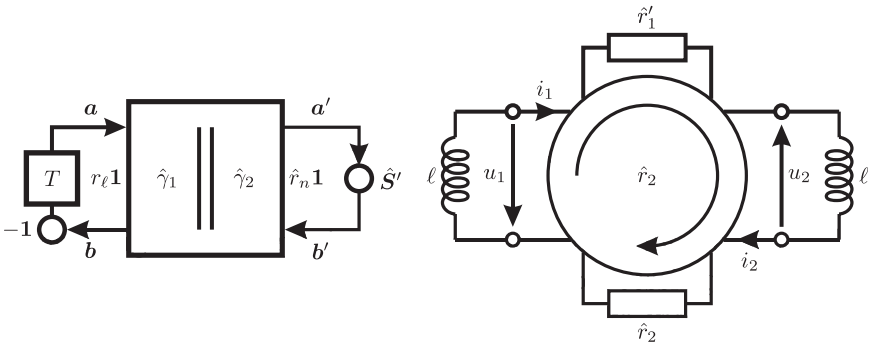

Figure 9. Left: A wave digital structure for a state-space model with a real eigenvalue of algebraic multiplicity n and geometric multiplicity 1. Right: The corresponding electrical circuit for two states.

At a simulation instance, we know all a_v from the delay elements and from $\hat{\mathbf{S}}'$ we deduce $b'_{\mathrm{n}} = 0$. Then, for $v = n, \ldots, 2$, one computes the equations of the parallel adaptor

$$\begin{bmatrix} b_v \\ a'_v \end{bmatrix} = \begin{bmatrix} \hat{\gamma}_1^2 - 1 & \hat{\gamma}_2\hat{\gamma}_1 \\ \hat{\gamma}_1\hat{\gamma}_2 & \hat{\gamma}_2^2 - 1 \end{bmatrix} \begin{bmatrix} a_v \\ b'_v \end{bmatrix}$$

and exploits the special structure of the scattering matrix:

$$b'_{v-1} = -\hat{\varrho}\,[a'_v + b'_v]$$

The new values of the delay elements are given by $-b_v$. As we can take from Figure 9 for $n = 2$ states, $\hat{S}' = \hat{\mathbf{S}}_J$ is the scattering matrix of a circulator terminated by the resistances $\hat{r}'_1 = \hat{r}_2\,[1 + \hat{\varrho}]/[1 - \hat{\varrho}]$ and $\hat{r}_2$.

To examine this state-space model with regard to passivity, it is instructive to choose

$$\hat{a}(t) = -\frac{\Omega}{2}\frac{2 + \Omega^2 t^2}{1 + \Omega^2 t^2} \Rightarrow \psi(t) = \exp\left(-\frac{\Omega t}{2} - \frac{\arctan(\Omega t)}{2}\right) \tag{54}$$

In view of Equation (12) it is evident that for any initial state and any finite initial instance the states tend towards zero for $t \to \infty$. Hence, the system is said to be asymptotic stable in the sense of Lyapunov [19]. Despite that stability property, one easily checks with the aid of the recurrence formula (51) and

$$r_{\mathrm{a}} = \ell\frac{\Omega}{2} > 0, \quad \hat{r}_n = r_a\frac{2 + \Omega^2 t^2}{1 + \Omega^2 t^2} > r_a \tag{55}$$

that the system is not passive for $n > 2$, because the resistances $\hat{r}_\mu$ are positive only for $n \leqslant 2$.

6. WAVE DIGITAL MODEL OF A NONLINEAR OSCILLATOR

At last, a wave digital model is derived for nonlinear oscillators obeying the second-order nonlinear and time-variant differential equation

$$\ddot{\vartheta} + \Omega_{\mathrm{s}}\hat{f}(\vartheta, \dot{\vartheta}, t)\,\dot{\vartheta} + \Omega_{\mathrm{a}}^2\,\hat{g}(\vartheta) = 0 \;\text{ with } \Omega_{\mathrm{s}} \geqslant 0 \;\text{ and }\; \Omega_{\mathrm{a}} > 0 \tag{56}$$

where $\hat{f}$ as well as $\hat{g}$ characterize the nonlinearity of the oscillator. This differential equation covers a variety of nonlinear oscillators, especially those that have successfully been used for

DOI: 10.1002/jnm

wave digital simulations like the well-known gravity pendulum, the Van der Pol and Duffing oscillator, cf. [6, 7, 23]. In comparison to the last examples, this situation is special in so far as we are now faced with a nonlinear differential equation being of second order instead of having an appropriate state-space model containing two differential equations of first order. Now, it is the aim to derive a reference circuit by converting the differential equation (56) into the form

$$\ell \frac{\mathrm{d}}{\mathrm{d}t}\mathbf{i} + \hat{\mathbf{Z}}_\mathrm{a}\mathbf{i} + \hat{\mathbf{Z}}_\mathrm{s}\mathbf{i} = \mathbf{0} \;\text{ with } n = 2 \tag{57}$$

This problem can be tackled by performing the following four steps:

1 First of all, we rewrite the nonlinear function $\hat{g}$ as

$$\hat{g}(\vartheta) = \hat{h}(\vartheta)\hat{h}'(\vartheta) \;\text{ with } \hat{h}^2(\vartheta) = 2\int \hat{g}(\vartheta)\,\mathrm{d}\vartheta + \text{const} \tag{58}$$

and notice that both systems have the same power balance:

$$\dot{\vartheta}\frac{\mathrm{d}}{\mathrm{d}t}\dot{\vartheta} + \Omega_\mathrm{s}\hat{f}(\vartheta,\dot{\vartheta},t)\,\dot{\vartheta}^2 + \Omega_\mathrm{a}^2\,\hat{h}(\vartheta)\frac{\mathrm{d}}{\mathrm{d}t}\hat{h}(\vartheta) = \mathbf{i}^\mathrm{T}\ell\frac{\mathrm{d}}{\mathrm{d}t}\mathbf{i} + \mathbf{i}^\mathrm{T}\hat{\mathbf{Z}}_\mathrm{s}\mathbf{i} \tag{59}$$

2 The latter equality must hold even in the lossless case $\Omega_\mathrm{s} = \mathbf{0}$ and $\hat{\mathbf{Z}}_\mathrm{s} = \mathbf{0}$, from which it appears natural to assign the state variables

$$i_1 = \frac{\dot{\vartheta}}{\sqrt{\ell}} \;\text{ and }\; i_2 = \frac{\Omega_\mathrm{a}}{\sqrt{\ell}}\,\hat{h}(\vartheta) \tag{60}$$

3 With the definition of the currents, we are able to determine the antimetric part of the resistance matrix by exploiting the differential equation (56) in the lossless case:

$$\ell\frac{\mathrm{d}}{\mathrm{d}t}\mathbf{i} + \hat{\mathbf{Z}}_\mathrm{a}\mathbf{i} = \mathbf{0} \Rightarrow \hat{r}_{21} = -\ell\Omega_\mathrm{a}\,\hat{h}'(\vartheta) \tag{61}$$

4 At last, we incorporate possible losses. The equality of the power balances (59) leads to the additional requirement

$$\Omega_\mathrm{s}\hat{f}(\vartheta,\dot{\vartheta},t)\,\dot{\vartheta}^2 = \mathbf{i}^\mathrm{T}\hat{\mathbf{Z}}_\mathrm{s}\mathbf{i} \tag{62}$$

which is met by the choice

$$\hat{r}_1 = \ell\Omega_\mathrm{s}\hat{f}(\vartheta,\dot{\vartheta},t),\quad \hat{r}_2 = 0,\ \hat{n}_{21}\text{ arbitrary} \tag{63}$$

Hence, all elements of the reference circuit are specified and the corresponding wave digital model is basically the one of Figure 8, where the wave digital equivalent of the resistance $\hat{r}_2$ and its interconnected series adaptor can be omitted. In case of a lossless oscillator, the resistance matrix $\hat{\mathbf{Z}}$ corresponds to a complex-valued scalar state-space model, with $\hat{Z} = j\hat{r}_{21}$. It has the efficient wave digital implementation depicted on the left-hand side of Figure 10, where the real and imaginary parts of the signals belong to those of the real wave digital structure with index 1 or 2, respectively.

DOI: 10.1002/jnm

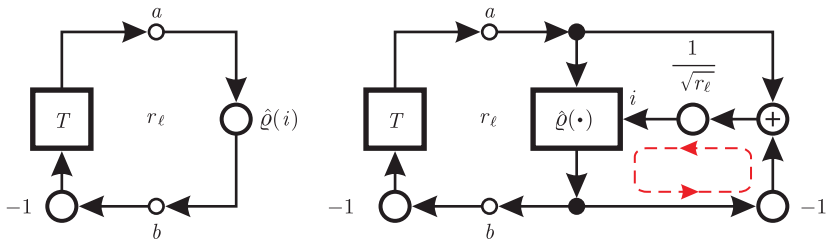

Figure 10. Wave digital model of a lossless oscillator (left), possessing a latent algebraic loop (right).

Unlike the time-variant case, these algorithms are not explicit, because they cover hidden implicit equations. These are caused by nonlinear algebraic relations and accordingly named algebraic loops here. For example, the lossless oscillator bears one algebraic loop, which is visualized on the right-hand side of Figure 10. These implicit equations have to be resolved within each simulation instance by using a numerical iteration technique, like fixed point iteration.

6.1. Analytical solution of the gravity pendulum

A state of the art example is a simple gravity pendulum without any friction, where the bob falls at an initial angle $\vartheta(t_0) = \vartheta_0$, with an initial angular velocity $\dot{\vartheta}(t_0) = \dot{\vartheta}_0$. It obeys the differential equation (56), with

$$\Omega_s = 0 \quad \text{and} \quad \hat{g}(\vartheta) = \sin(\vartheta). \tag{64}$$

In the absence of friction, the (normalized) energy of motion is constant and determined by the sum of the pendulum's initial kinetic and potential energy:

$$\dot{\vartheta}^2(t) + 4\Omega_a^2 \sin^2(\vartheta(t)/2) = E, \quad \text{with} \quad E = \dot{\vartheta}_0^2 + 4\Omega_a^2 \sin^2(\vartheta_0/2). \tag{65}$$

Evidently, if the angular velocity vanishes for an instance, the pendulum does not flip over and the energy is limited to maximum potential energy: $E < E_0 = 4\Omega_a^2$. For this scenario, there exists the solution [24]

$$\vartheta(t) = 2\arcsin(k\,\mathrm{sn}(\alpha(t), k)),\ \dot{\vartheta}(t) = \mathrm{sgn}(\dot{\vartheta}_0)\sqrt{E}\,\mathrm{cn}(\alpha(t), k),\ \alpha(t) = \alpha_1[t - t_0] + \alpha_0, \tag{66}$$

where sn and cn denote Jacobi elliptic functions [25], and

$$0 \leqslant k = \sqrt{E/E_0} < 1, \quad \alpha_1 = \mathrm{sgn}(\dot{\vartheta}_0)\Omega_a, \quad \alpha_0 = \mathrm{sn}^{-1}(k_0/k, k), \quad k_0 = \sin(\vartheta_0/2). \tag{67}$$

The angle and the angular velocity are periodic functions

$$\vartheta(t) = \vartheta(t - T_a), \quad \dot{\vartheta}(t) = \dot{\vartheta}(t - T_a), \tag{68}$$

where the period T_a can be calculated from the complete elliptic integral K. The latter is a function of the modulus k and can be expressed by the inverse elliptic function sn^{-1}:

$$\Omega_a T_a = 4K(k), \quad \text{with} \quad K(k) = \mathrm{sn}^{-1}(1, k) = \int_0^1 \frac{\mathrm{d}\zeta}{\sqrt{[1 - \zeta^2][1 - k^2\zeta^2]}} \tag{69}$$

Fig. 11 shows the solution of the angle and its derivative for a gravity pendulum with $\Omega_a = 1/\mathrm{s}$, $\vartheta_0 = \pi 179.9/180$, and $\dot{\vartheta}_0 = 0/\mathrm{s}$. Here, the time axes are scaled with respect to the period T_a and $\vartheta_{\max} = -\vartheta_{\min} = \vartheta_0$. Because of insufficient energy the pendulum cannot flip over, which implies

DOI: 10.1002/jnm

the following restrictions for the angle and angular velocity, respectively:

$$\vartheta_{\min} \leqslant \vartheta(t) \leqslant \vartheta_{\max} \quad \text{with} \quad \vartheta_{\max} = -\vartheta_{\min} = 2\,\mathrm{Arcsin}(k) < \pi, \tag{70a}$$

$$\dot{\vartheta}_{\min} \leqslant \dot{\vartheta}(t) \leqslant \dot{\vartheta}_{\max} \quad \text{with} \quad \dot{\vartheta}_{\max} = -\dot{\vartheta}_{\min} = \sqrt{E}. \tag{70b}$$

A whirling pendulum has an energy E greater than E_0, which is equivalent to $k>1$. In this situation the solution of [24] can essentially be used, but elliptic functions are commonly numerically implemented for $0<k<1$ only. To overcome this, we apply a reciprocal modulus transformation [25]:

$$\chi = 1/k, \quad \mathrm{sn}(\zeta, k) = \chi \mathrm{sn}(k\,\zeta, \chi), \quad \mathrm{cn}(\zeta, k) = \mathrm{dn}(k, \zeta, \chi, \quad \alpha_0 = \chi \mathrm{sn}^{-1}(k_0, \chi), \tag{71}$$

where dn designates another Jacobi elliptic function. This leads to

$$\vartheta(t) = 2\,\arcsin(\mathrm{sn}(k\,\alpha(t), \chi))\mathrm{sgn}(\mathrm{cn}(k\,\alpha(t), \chi)), \quad \dot{\vartheta}(t) = \mathrm{sgn}(\dot{\vartheta}_0)\sqrt{E}\mathrm{dn}(k\,\alpha(t), \chi) \tag{72}$$

The expression $\mathrm{sgn}(\mathrm{cn}(k\ \alpha(t),\chi))$ solely commutates the sign of the angle in a suited manner, because we have to consider that the pendulum does not swing back, which implies a constant sign of the angular velocity. The periodicity of the angle and the angular velocity holds true, but we have to modify the period:

$$\vartheta(t) = \vartheta(t - T_\mathrm{a}), \quad \dot{\vartheta}(t) = \dot{\vartheta}(t - T_\mathrm{a}), \quad \Omega_\mathrm{a} T_\mathrm{a} = 2K(k) = 2\chi K(\chi). \tag{73}$$

The angle is of course limited to $|\vartheta| \leqslant \pi$ and the angular velocity obeys

$$\dot{\vartheta}_{\min} \leqslant \mathrm{sgn}(\dot{\vartheta}_0)\dot{\vartheta}(t) \leqslant \dot{\vartheta}_{\max} \text{ with } \dot{\vartheta}_{\min} = \sqrt{E - E_0} \text{ and } \dot{\vartheta}_{\max} = \sqrt{E}. \tag{74}$$

Since the angular velocity is the time derivative of the angle, we finally have to unwrap the angle by adding multiples of 2π as it is shown in Fig. 12 for a whirling pendulum, with $\Omega_\mathrm{a} = 1/\mathrm{s}$, $\vartheta_0 = \pi 179.9/180$, and $\dot{\vartheta}_0 = 0.1667/\mathrm{s}$.

6.2. *Wave digital model of the gravity pendulum*

In this subsection, we briefly discuss a complex valued wave digital modeling of the gravity pendulum, for which we deduce the following three functions from the differential equation:

$$\hat{g}(\vartheta) = \sin(\vartheta) \Rightarrow \hat{h}(\vartheta) = 2\,\sin(\vartheta/2) \Rightarrow \hat{h}'(\vartheta) = \cos(\vartheta/2) \tag{74}$$

In order to avoid a renewed discussion about case differentiations if the pendulum turns over, let us restrict the explanation to $|\vartheta| < \pi$. Under this restriction $\hat{h}$ is uniquely invertible and the

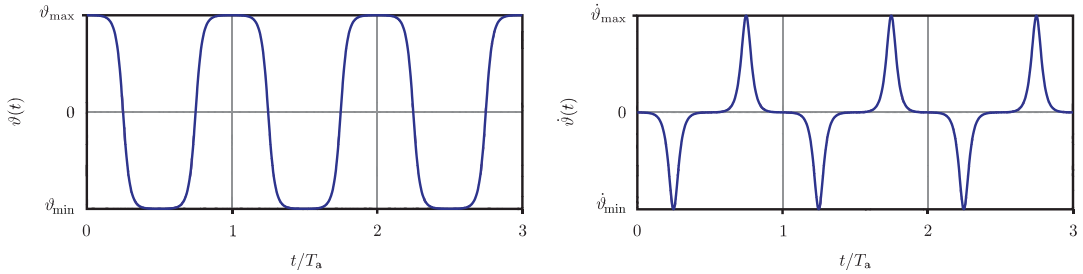

Figure 11. Angle (left) and angular velocity (right) of a pendulum, which is not turning over.

DOI: 10.1002/jnm

Equation (60) leads under consideration of $i = i_1 + \mathrm{j}i_2$ to the expressions

$$\vartheta(t) = 2\,\mathrm{Arcsin}\left(\frac{\sqrt{\ell}\,\mathrm{Im}^2\,\{i(t)\}}{2\Omega_\mathrm{a}}\right),\quad \dot{\vartheta}(t) = \sqrt{\ell}\,\mathrm{Re}\{i(t)\} \tag{75}$$

for the angle and its derivative, respectively. Hence, the complex-valued resistance as well as the reflection coefficient depend on the current

$$\begin{aligned}\hat{Z}(i) &= \mathrm{j}\hat{r}_{21}(i) = -\ell\Omega_\mathrm{a}\hat{h}'(\vartheta) = -\mathrm{j}\ell\Omega_\mathrm{a}\sqrt{\frac{1-\ell\,\mathrm{Im}^2\,\{i\}}{4\Omega_\mathrm{a}^2}}\\ \hat{\varrho}(i) &= \frac{\hat{Z}(i)-r_\ell}{\hat{Z}(i)+r_\ell}\end{aligned} \tag{76}$$

On the other side, the current is a linear combination of the power waves depending on the reflection coefficient. This in turn causes the implicit equation

$$i = [1-\hat{\varrho}(i)]a/\sqrt{r_\ell} \tag{77}$$

in accordance to the algebraic loop of Figure 10. Note that this model can also be extended to a whirling pendulum. A wave digital simulation of the pendulum reproduces the angle and the angular velocity of the Figures 11 and 12. For a step size of $T = 10\,\mathrm{ms}$ and only 1 fixpoint iteration step, the relative error is about 1%. Moreover, due to losslessness, the reflection coefficient satisfies $|\hat{\varrho}| = 1$, implying constant absolute values of the power waves and it suffices to numerically compute their phases: instead of a multiplication with the reflection coefficient, we simply have to add its corresponding phase to those of the power waves. This way, rounding errors affect only phases, whereas the absolute values remain unchanged. As a consequence, even under finite-arithmetic conditions the initial energy is exactly preserved by the numeric model. To verify this, one can find the trajectories of two wave digital simulation results in Figures 13. Although simulations have been done for 100 periods, energy is conserved during the simulations.

Generally, rounding errors could produce or dissipate energy and hence drive or damp the pendulum, which makes an undesired chaotic behavior possible, if the pendulum turns sometimes over or not. Following the above arguments, this is impossible for the present wave digital model. Hence, it is perfectly suited for emulating a nonlinear oscillator in continuously running real-time applications.

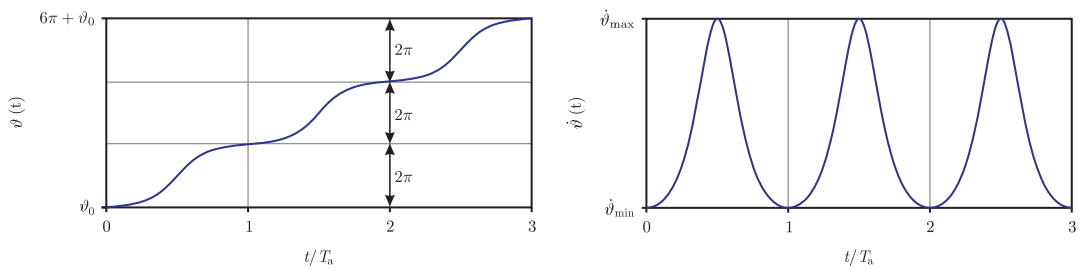

Figure 12. Unwrapped angle (left) and angular velocity (right) of a whirling pendulum.

DOI: 10.1002/jnm

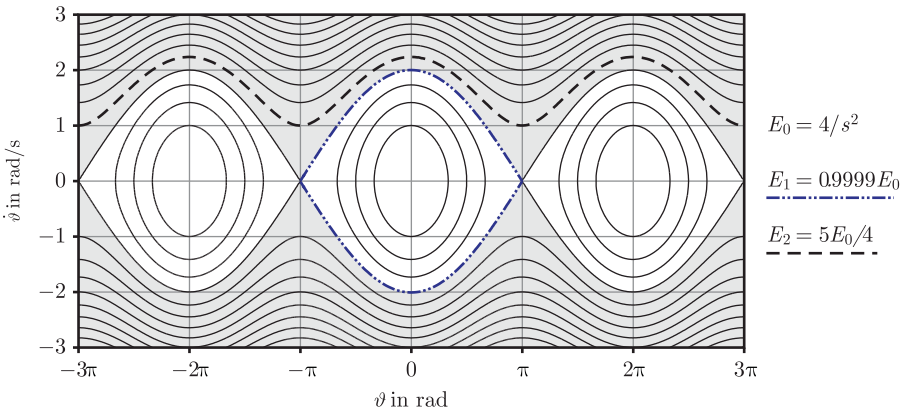

Figure 13. Trajectories in the phase space $\dot{\vartheta}$ vs. ϑ, with lines of constant energy. Regions of $E < E_0$ are white and those of $E > E_0$ are gray-shaded.

7. CONCLUSIONS

In this paper, an internally passive electrical circuit has been derived for a special class of passive state-space models. The differential operator is constituted by voltage-current relations of inductances and parameters are represented in terms of resistances, turns ratios, and gyration resistances. This way, structural information has been acquired and the values of the electrical devices give information about the behavior of the electrical circuit and thus about the abstract differential equations system. Moreover, a systematic approach for finding a realizable wave digital model has been presented. This approach has been verified for time-variant as well as nonlinear differential equations, by comparing simulation results with analytical solutions.

REFERENCES

1. Fettweis A. Digital filters related to classical filter networks. *AEÜ International Journal of Electronics and Communication* 1971; **25**(2):79–89.
2. Fettweis A, Meerkötter K. On parasitic oscillations in digital filters under looped conditions. *IEEE Transactions on Circuits and Systems* 1977; **24**:475–481.
3. Fettweis A. Wave digital filters: theory and practice. *Proceedings of the IEEE* 1986; **74**(2):270–327.
4. Fettweis A. Robust numerical integration using wave-digital concepts. *Multidimensional Systems and Signal Processing* 2006; **17**(1):7–25.
5. Meerkötter K, Scholz R. Digital simulation of nonlinear circuits by wave digital filter principles. *Proceedings IEEE International Symposium on Circuits and Systems*, Portland, OR, vol. I, 1989; 720–723.
6. Felderhoff T. Simulation of nonlinear circuits with periodic doubling and chaotic behavior by wave digital filter principles. *IEEE Transactions on Circuits and Systems* 1994; **41**(1):485–491.
7. Felderhoff T. A new wave description for nonlinear elements. *Proceeding IEEE International Symposium on Circuits and Systems* (*ISCAS*), Atlanta, GA, U.S.A., vol. 3, 1996; 221–224.
8. Petrausch S, Rabenstein R. Wave digital filters with multiple nonlinearities. *12th European Signal Processing Conference* (*EUSIPCO*), vol. 47(6), 2004; 77–80.
9. Fettweis A, Nitsche G. Numerical integration of partial differential equations by means of multidimensional wave digital filters. *Proceeding IEEE International Symposium on Circuits and Systems* (*ISCAS*), vol. II. 1990; 954–957.
10. Fettweis A, Nitsche G. Numerical integration of partial differential equations using principles of multidimensional wave digital filters. *Journal of VLSI Signal Processing* 1991; **3**(1/2):7–24.
11. Fettweis A. Discrete modelling of lossless fluid dynamic systems. *AEÜ International Journal of Electronics and Communication* 1992; **46**:209–218.

DOI: 10.1002/jnm

12. Fränken D, Meerkötter K, Waßmuth J. Observer-based feedback linearization of dynamic loudspeakers with AC amplifiers. *IEEE Transactions on Speech and Audio Processing* 2005; **13**(2):233–242.
13. Luhmann K, Ochs K. A novel interpretation of the hyperbolization method used to solve the parabolic neutron diffusion equations by means of the wave digital concept. *International Journal of Numerical Modelling: Electronic Networks, Devices and Fields* 2006; **19**(4):345–364.
14. Vollmer M. Numerical integration of PDEs for safety critical applications implemented by I&C systems. *Computer Safety*, *Reliability*, *and Security*, *23rd International Conference*, *SAFECOMP*, 2004: 269–282.
15. Fettweis A. Realizability of digital filter networks. *AEÜ International Journal of Electronics and Communication* 1976; **30**(2):90–96.
16. Belevitch V. *Classical Network Theory*. Holden-Day: San Francisco, CA 1968.
17. Willems JC. Dissipative dynamical systems, part I: General theory; part II: linear systems with quadratic supply rates. *Archive for Rationale Mechanics Analysis* 1972; **45**:321–393.
18. Wyatt JL *et al*. Energy concepts in the state space theory of nonlinear n-ports: Part I- passivity. *IEEE Transactions on Circuits and Systems* 1981; **28**(1):48–61.
19. Kailath T. *Linear Systems* (*Prentice Hall Information and System Science Series*). Prentice-Hall: Englewood cliffs, NJ, 1980.
20. Meerkötter K, Fränken D. Digital realization of connection networks by voltage-wave two-port adaptors. *AEÜ International Journal of Electronics and Communication* 1996; **50**:362–367.
21. Fränken D. *Digitale Simulation physikalischer Systeme mit Methoden der Netzwerktheorie* (*Fortschritt-Berichte VDI*). VDI Verlag: Dusseldorf, 2003.
22. Fränken D, Ochs J, Ochs K. Generation of wave digital structures for networks containing multiport elements. *IEEE Transactions on Circuits and Systems, Part I*: *Regular Papers* 2005; **52**(3):586–596.
23. Ochs K. Passive integration methods: fundamental theory. *AEÜ International Journal of Electronics and Communication* 2001; **55**(3):153–163.
24. Belendez A *et al*. Exact solution for the nonlinear pendulum. *Revista Brasileira de Ensino Fisica* 2007; **29**(4):645–648.
25. Byrd PF, Friedmann MD. *Handbook of Elliptical Integrals for Engineers and Scientists*. Springer: Belrin 1971.

AUTHORS' BIOGRAPHY

Karlheinz Ochs was born in Lingen, Germany, in 1968. He received the Dipl Ing degree and the Dr Ing degree in Electrical Engineering both from the University of Paderborn, Germany, in 1996 and 2001, respectively. From 2001 to 2002, he was a design engineer at the Technology and Development Center, Siemens AG, Bruchsal, Germany. Currently, he is a postdoctoral researcher at the Department of Electrical Engineering and Information Technology/Communications Engineering at the Ruhr-University, Bochum, Germany. Research interests include digital signal processing and transmission.

DOI: 10.1002/jnm